Protist, Vol. 170, 125698, December 2019
http://www.elsevier.de/protis
Published online date 1 November 2019

Protist

ORIGINAL PAPER

Quantitative Proteomic Map of the Trypanosomatid *Strigomonas culicis*: The Biological Contribution of its Endosymbiotic Bacterium

Giselle V.F. Brunoro[a,2], Rubem F.S. Menna-Barreto[b,2], Aline S. Garcia-Gomes[a,c,d,2], Carolina Boucinha[d], Diogo B. Lima[e,3], Paulo C. Carvalho[e], André Teixeira-Ferreira[a], Monique R.O. Trugilho[a], Jonas Perales[a], Veit Schwämmle[f], Marcos Catanho[g], Ana Tereza R. de Vasconcelos[h], Maria Cristina M. Motta[i], Claudia M. d'Avila-Levy[d,1,4], and Richard H. Valente[a,1]

[a]Laboratory of Toxinology, IOC, Oswaldo Cruz Foundation (FIOCRUZ), Rio de Janeiro, RJ 21040-900, Brazil
[b]Laboratory of Cellular Biology, IOC, Oswaldo Cruz Foundation (FIOCRUZ), Rio de Janeiro, RJ 21040-900, Brazil
[c]Laboratório de Microbiologia, Instituto Federal de Educação, Ciência e Tecnologia do Rio de Janeiro (IFRJ), Departamento de Alimentos, Rio de Janeiro, RJ 20270-021, Brazil
[d]Laboratory of Integrated Studies in Protozoology, IOC, Oswaldo Cruz Foundation (FIOCRUZ), Rio de Janeiro, RJ 21040-900, Brazil
[e]Laboratory for Structural and Computational Proteomics, ICC, Oswaldo Cruz Foundation (FIOCRUZ), Paraná, PR 81350-010, Brazil
[f]Department for Biochemistry and Molecular Biology, University of Southern Denmark, Odense 5230, Denmark
[g]Laboratory of Molecular Genetics of Microrganisms, IOC, Oswaldo Cruz Foundation (FIOCRUZ), Rio de Janeiro, RJ 21040-900, Brazil
[h]National Laboratory for Scientific Computing, Petrópolis, RJ 25651-075, Brazil
[i]Laboratório de Ultraestrutura Celular Hertha Meyer, Instituto de Biofísica Carlos Chagas Filho, Universidade Federal do Rio de Janeiro (UFRJ), Rio de Janeiro, RJ 21491-590, Brazil

Submitted May 17, 2019; Accepted October 20, 2019
Monitoring Editor: Dmitri Maslov

[1]Corresponding authors;
[2]These authors contributed equally to this work.
[3]Present address: Mass Spectrometry for Biology Unit, CNRS, USR 2000, Institut Pasteur, Paris 75015, France
[4]Present temporary address: de Duve Institute, Université Catholique de Louvain, Brussels 1200, Belgium
e-mails davila.levy@gmail.com (C.M. d'Avila-Levy), richardhemmi@gmail.com (R.H. Valente).

Abbreviations: SC, *Strigomonas culicis*; CKB, *Candidatus* Kinetoplastibacterium blastocrithidii; CKC, *Candidatus* Kinetoplastibacterium crithidii; WT, Wild type; Apo, Aposymbiotic; lag phase, Well-defined adaptation phase; log phase, Exponential phase; GO, Gene Ontology; ETS, Electron transport system; ROS, Reactive oxygen species; LIT, Liver infusion and tryptose medium; PSM, Peptide-spectrum matching.

https://doi.org/10.1016/j.protis.2019.125698

Strigomonas culicis **is a kinetoplastid parasite of insects that maintains a mutualistic association with an intracellular symbiotic bacterium, which is highly integrated into the protist metabolism: it furnishes essential compounds and divides in synchrony with the eukaryotic nucleus. The protist, conversely, can be cured of the endosymbiont, producing an aposymbiotic cell line, which presents a diminished ability to colonize the insect host. This obligatory association can represent an intermediate step of the evolution towards the formation of an organelle, therefore representing an interesting model to understand the symbiogenesis theory. Here, we used shotgun proteomics to compare the *S. culicis* endosymbiont-containing and aposymbiotic strains, revealing a total of 11,305 peptides, and up to 2,213 proteins (2,029 and 1,452 for wild type and aposymbiotic, respectively). Gene ontology associated to comparative analysis between both strains revealed that the biological processes most affected by the elimination of the symbiont were the amino acid synthesis, as well as protein synthesis and folding. This large-scale comparison of the protein expression in *S. culicis* marks a step forward in the comprehension of the role of endosymbiotic bacteria in monoxenous trypanosomatid biology, particularly because trypanosomatids expression is mostly post-transcriptionally regulated.**

Key words: *Strigomonas culicis*; endosymbiont-bearing trypanosomatid; proteomics; amino acid and protein syntheses; protein folding; energy metabolism.

Introduction

The Trypanosomatidae family (Kinetoplastea: Trypanosomatida) comprises parasites of vertebrates, invertebrates or plants. From the more than 20 formally described genera, two display species that are the causative agents of Chagas disease (*Trypanosoma cruzi*), several types of leishmaniases (*Leishmania* spp.), and Human African Trypanosomiasis (*Trypanosoma brucei* sensu lato). These parasites alternate their life cycles between an insect vector and a mammalian host, affecting ca. 22 million people worldwide (Rodrigues et al. 2014). Nonetheless, the largest biodiversity of this protist family is among trypanosomatids that usually carry out their entire life cycle in insects (D'Avila-Levy et al. 2015; Maslov et al. 2019).

Among insect trypanosomatids, members of the Strigomonadinae subfamily form a monophyletic clade composed of the genera *Angomonas*, *Strigomonas*, and *Kentomonas*, which have in common the presence of an endosymbiotic β-proteobacterium, *Candidatus* Kinetoplastibacterium spp. (Maslov et al. 2013; Teixeira et al. 2011; Votýpka et al. 2014). Recently, a new kinetoplastidbacterium association has been reported for another trypanosomatid species (*Novymonas esmeraldas*); however, it is evolutionarily and phylogenetically divergent, when compared to the members of the Strigomonadinae subfamily, and probably configures a completely different biological interaction (Kostygov et al. 2016, 2017). Bacterial endosymbionts play a critical role in eukaryote evolution, which is illustrated by the widespread occurrence of mitochondria and plastids, organelles that have a symbiogenetic origin (López-García et al. 2017; Margulis and Bermudes 1985). The endosymbiosis in trypanosomatids is a mutualistic association and this intricate interaction possesses several characteristics which probably configure an intermediate step of the evolution towards the formation of an organelle (de Souza and Motta 1999; Harmer et al. 2018; Motta 2010; Motta et al. 2013; Yurchenko and Lukeš 2018). Therefore, it is not surprising that the first description of an endosymbiont, as diplosomes in *Strigomonas culicis* (Novy et al. 1907), propelled the research in endosymbiont-harboring trypanosomatids.

Another fact that also furthered symbiosis research in trypanosomatids is the possibility of bacteria removal by antibiotic treatment, which allows the obtainment of aposymbiotic strains that can be maintained only in vitro. Such cured cells can be used as comparative models to understand how the symbiont influences the host trypanosomatid structure and physiology (Bombaça et al. 2017; Chang and Trager 1974; D'Avila-Levy et al. 2005a, b; Loyola-Machado et al. 2017; Motta 2010; Yurchenko and Lukeš 2018). Up to now, all attempts to cultivate the bacteria alone have demonstrated that these endosymbionts have a strict dependence on the protist host, being unable to survive outside the trypanosomatids (reviewed in Motta 2010). Trypanosomatids from the subfamily Strigomonadinae bear only a single bacterium in the cytoplasm, which is vertically transmitted after a synchronous division with the host cell. The intracellular localization of the bacterium is not random, being closely associated to the cellular nucleus and surrounded

by glycosomes (Brum et al. 2014; Catta-Preta et al. 2015; Loyola-Machado et al. 2017; Motta et al. 2010). The presence of the endosymbiont in trypanosomatids is related to morphological alterations in the cytoskeleton, kinetoplast, and paraflagellar rod of the host cell (Freymuller and Camargo 1981; Gadelha et al. 2005; Votýpka et al. 2014).

The endosymbiont-trypanosomatid interaction is characterized by intense metabolic exchange (Alfieri and Camargo 1982; Camargo and Freymuller 1977; Chang et al. 1975; Chang and Trager 1974), which has been recently characterized at genomic level (Alves et al. 2011, 2013a; Klein et al. 2013; Kořený et al. 2010; Motta et al. 2013; Votýpka et al. 2014). In spite of considerable genome reduction in the bacterium, it maintains genes responsible for the biosynthesis of compounds essential for the host, either providing precursor molecules or complementing indispensable biosynthetic pathways, such as those for amino acids, vitamins, cofactors, lipids, and the purine/pyrimidine (Alves et al., 2013a, b; Azevedo-Martins et al. 2015; Klein et al. 2013; Motta et al. 2013). The symbiont from *Kentomonas sorsogonicus* presents a smaller genome than other ca. Kinetoplastibacterium spp., having even lost the heme-synthesis pathway, once considered as a hallmark of endosymbionts in trypanosomatids (Silva et al. 2018).

Although trypanosomatids cured of their endosymbionts can proliferate in culture media, they are unable to colonize the insect host (Bombaça et al. 2017; Corrêa-da-Silva et al. 2006; Fampa et al. 2003) and present a more fermentative metabolism (Bombaça et al. 2017; Loyola-Machado et al. 2017). Nevertheless, in vivo administration of the antioxidant ascorbate in *Aedes aegypti* midgut led to a reduction in oxidative stress, allowing insect colonization by this strain. Hence, the authors inferred that the lack of a properly functioning natural antioxidant system could account for *S. culicis* aposymbiotic strain's inability to colonize the insect host (Bombaça et al. 2017). Additionally, alterations in the exposure of surface carbohydrates, peptidases and ecto-phosphatases, as well as changes in the overall surface charge in aposymbiotic strains could explain their inability to adhere and colonize the insect host (Catta-Preta et al. 2013; D'Avila-Levy et al. 2005a, b, 2008; de Oliveira et al. 2015; Dwyer and Chang 1976; Esteves et al. 1982; Fampa et al. 2003; Oda et al. 1984).

Genome sequencing and determination of transcriptome content of symbiont-bearing trypanosomatids have provided a significant improvement in the understanding of this mutualistic association (Motta et al. 2013; Penha et al. 2016). Additionally, the overall protein profile has never been assessed and, considering that trypanosomatids expression is post-transcriptionally regulated, protein analysis is of outmost relevance (Brunoro et al. 2015; Clayton and Shapira 2007; Parodi-Talice et al. 2004). Here, we applied shotgun proteomics to compare endosymbiont-bearing (wild type) and endosymbiont-free (aposymbiotic) strains of *S. culicis*, aiming at a better understanding of this intricate association.

Results

Ultrastructural and Phylogenetic Analyses of *S. culicis* Wild Type (WT) and Aposymbiotic (Apo) Strains

Inspection of the axenic cultures of each strain of *S. culicis* by electron microscopy reinforced the presence of the symbiont only in WT and confirmed previous observation on the ultrastructural impact of the artificial removal of the symbiont by antibiotic treatment (Freymuller and Camargo 1981; Fig. 1). The gGAPDH gene sequencing revealed 100% identity over 725 nucleotides among COLPROT034, COLPROT041, and a public sequence from *S. culicis* - ATCC 30268, EU079137. The Bayesian phylogenetic tree reconstructed using gGAPDH sequences was consistent with previously published tree that employed concatenated analysis with gGAPDH and 18S (Ishemgulova et al., 2017) (Fig. 2), thus confirming the positioning of the trypanosomatids analyzed herein as members of the Strigomonadinae subfamily.

Growth Curves and Time Points Selection for Proteomic Analysis

The growth curve for each strain of *S. culicis* was determined to pinpoint the times for protein identification and to guide data interpretation and analysis. WT strain demonstrated well-defined adaptation (lag) and exponential (log) phases, reaching maximum growth at 80 h, followed by a fast decrease in protist proliferation, without the establishment of a stationary phase. On the other hand, the aposymbiotic (Apo) strain presented a prolonged lag phase up to 56 h, when a clear log phase started, and the maximum growth peak was reached at 96 h, which was subsequently followed by a stationary phase (Fig. 3). Under the same culture conditions,

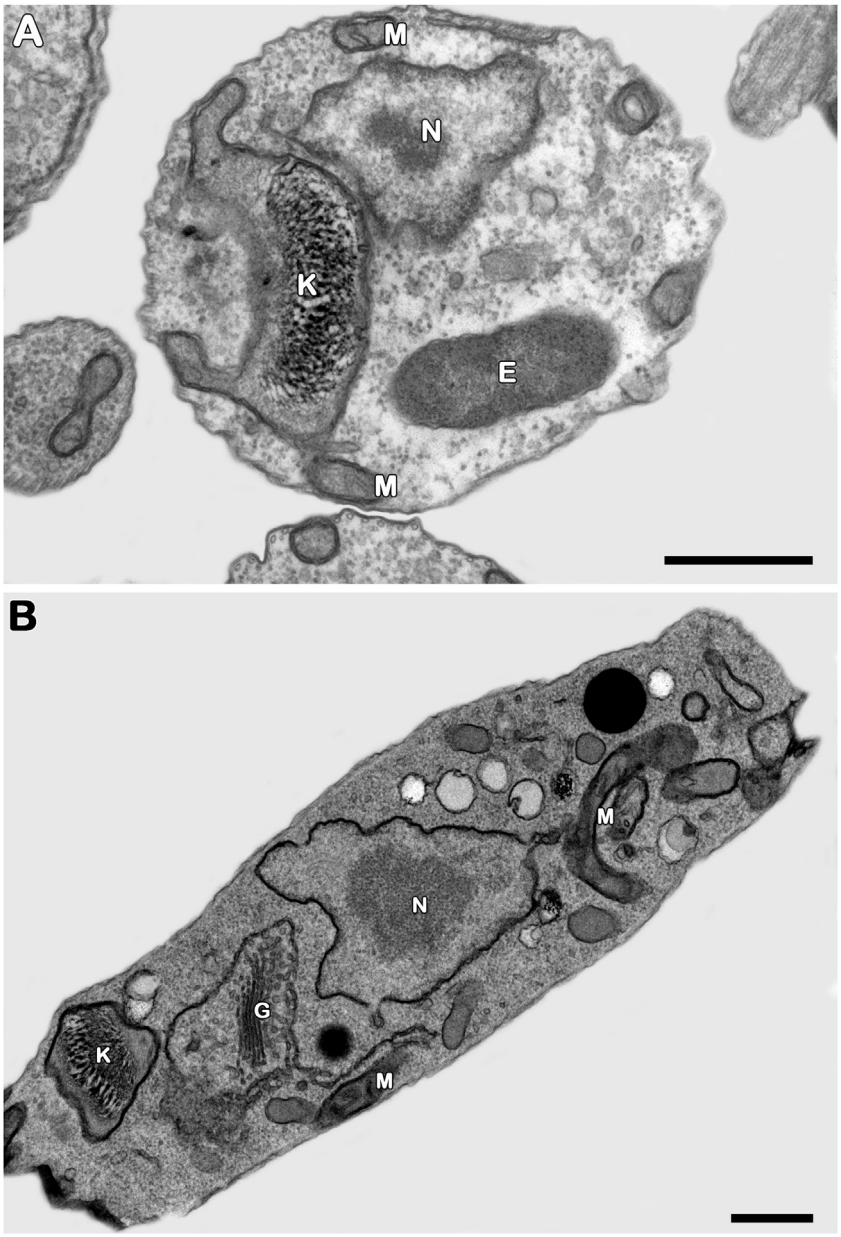

Figure 1. Ultrastructural evaluation of *S. culicis* epimastigotes. (**A**) Wild type (WT) and (**B**) aposymbiotic (Apo) strains. Both cells present typical morphology, with the endosymbiont (E) exclusively found in WT strain. N: nucleus; K: kinetoplast; M: mitochondrion; G: Golgi. Images from panels A an B were acquired under different magnification but bars represent 500 nm in both cases.

the cells proliferated in distinct patterns. It has been previously shown that the supply of two times more fetal bovine serum to the Apo strain can produce growth patterns similar to wild type (Catta-Preta et al. 2013). Considering the potential impact of distinct growth stimulus on protein expression, we chose to provide the same growth conditions. At time points of 24, 56, and 80 h, samples from each strain were then collected for subsequent analysis. At these same time points and at 96 h, pH measurements of the culture media of WT and Apo strains were taken and no changes were detected, relatively to the medium without parasite growth (data not shown).

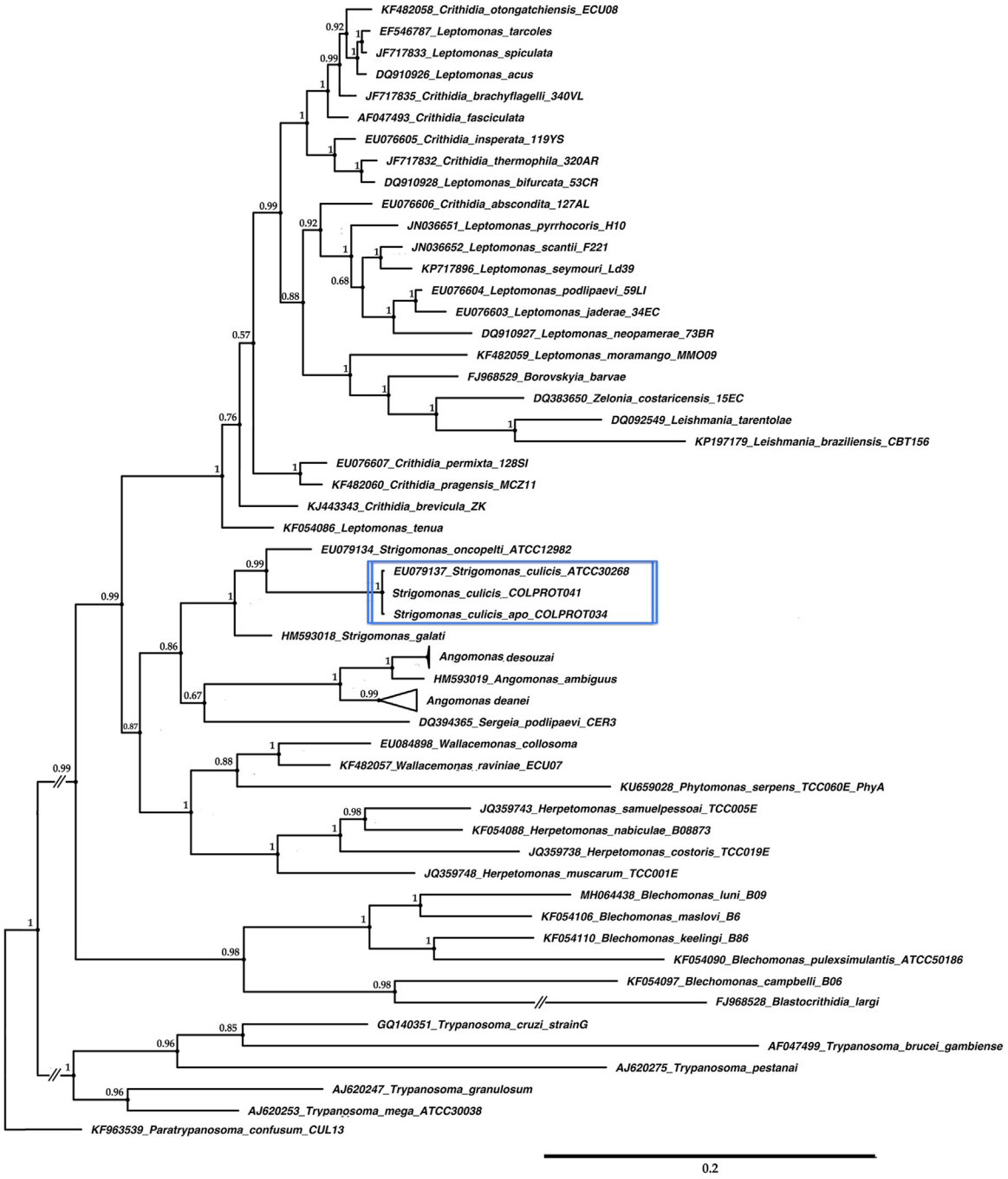

Figure 2. Bayesian inference tree based on the partial sequences of gGAPDH from *S. culicis* wild type (WT) and aposymbiotic (Apo) strains. The numbers at the top of each branch denote Bayesian posterior probability values. The tree was rooted with sequence of *Paratrypanosoma confusum*. Double-crossed branches are at 75% of their original lengths. The scale bar denotes the number of substitutions per site.

Qualitative Proteomic Analysis

The combined shotgun proteomics results from both strains identified 11,305 peptides, which corresponded to 2,213 proteins. A total of 2,029 proteins were identified for WT strain, whereas 1,452 were identified for Apo strain (sequenced by 9,433 and 5,975 peptides, respectively). *Ca*. Kinetoplastibacterium blastocrithidii (CKB) and *Ca.* K. crithidii (CKC) protein entries were identified in both WT

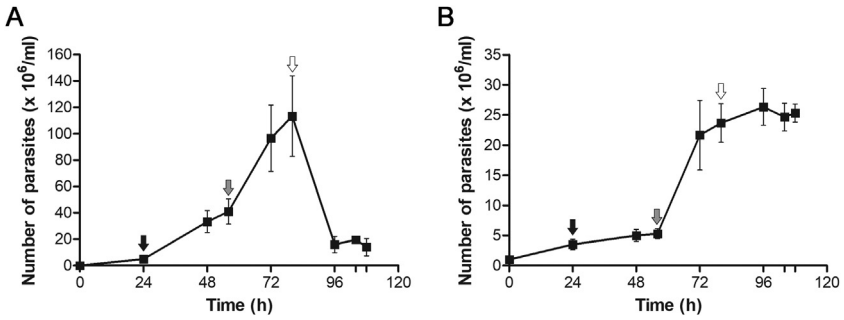

Figure 3. Proliferative behavior of *S. culicis*. Growth curves of (**A**) wild type (WT) and (**B**) aposymbiotc (Apo) strains. Experiment performed in three biological replicates (inocula from three independent cultures); data expressed as mean and standard deviation. Arrows indicate the time points selected for proteomic analysis: 24 h (black), 56 h (gray), and 80 h (white).

and Apo strains. However, they represented 6.64 % of the total spectral counts (8,877 out of 133,679) in WT strain, while only 0.15 % in Apo strain (174 out of 113,804), as expected (Supplementary Table A.1a-c). At these low levels, part of these spectra could be due to carry-over between WT and Apo samples, when analyzed by LC-MS/MS. Even if carry-over is not considered, one could roughly estimate that a cure ratio of 98 % was achieved for the Apo strain.

For each time point, the qualitative comparison showing the proteins that were observed in one or both strains, excluding the hypothetical proteins, is demonstrated in Figure 4 and Supplementary Table A.2a-h. After 24 h of growth, 198 and 72 proteins were exclusively detected in WT and Apo strains, respectively. At 56 h, these numbers were 131 and 250, and at 80 h, 224 and 40. The proportional Venn diagrams depicted the lowest overlap, between the two strains, of the overall protein content (26% - 131 out of 512 proteins) at the 56 h time point. According to the Gene Ontology (GO) (http://www.geneontology.org/) classification, the top-reported biological process, among the exclusively identified proteins in Apo at 24 h, was “carbohydrate metabolism”. At 56 h and 80 h, “translation (protein synthesis)” was the most reported (Supplementary Table A.3a-c). On the other hand, for WT strain, the top-reported process was “translation (protein synthesis)” for all time points studied (24 h, 56 h, and 80 h) (Supplementary Tables A.3d-f).

Additionally, the number of shared identifications at 24 h, 56 h, and 80 h (583, 131, and 115 common proteins, respectively – Fig. 4) presented a steadily decrease over time; these common identification lists were compared against each other (Supplementary Table A.4). The categories of shared biological processes throughout time points were acetyl-CoA biosynthetic process from pyruvate, ATP synthesis coupled proton transport, cell redox homeostasis, cellular amino acid metabolic process (biosynthetic process), gluconeogenesis and glycolytic process, protein folding and refolding, translation, tricarboxylic acid cycle, response to oxidative stress, ribosome biogenesis, and vesicle-mediated transport. Still, as the highest number of shared identifications occurred at 24 h, specific categories were shared only at this time point, being lost over time. These specific categories consist of tRNA synthetases and amino acid biosynthetic processes, carbohydrate metabolic process (pentose-phosphate shunt), DNA repair and replication, cilium assembly and cilium movement involved in cell motility, coenzyme A metabolic process and isoprenoid biosynthetic process, fatty acid biosynthetic process, peroxisome fission, proteolysis involved in cellular protein catabolic process, purine nucleotide biosynthetic process, and regulation of transcription and translation.

Quantitative Proteomic Analysis

The comparative analysis between both strains, at 24 h, showed that 13 proteins were more abundant in Apo strain, while 36 proteins were more abundant in WT strain (Table 1). At 56 h, 7 and 21 proteins showed higher abundance in Apo and WT strains, respectively. Finally, at 80 h, 12 and 24 proteins were more abundant in Apo and WT strains, respectively (Table 1). Hence, at all time points tested, WT strain presented higher numbers for more abundant proteins. Gene ontology categories such as amino acid and energy metabolism (including glycolysis, beta-oxidation, tricarboxylic acid cycle), cell signaling, and detoxification processes were clearly prominent in the presence of the symbiont (Supplementary Table A.5a-c).

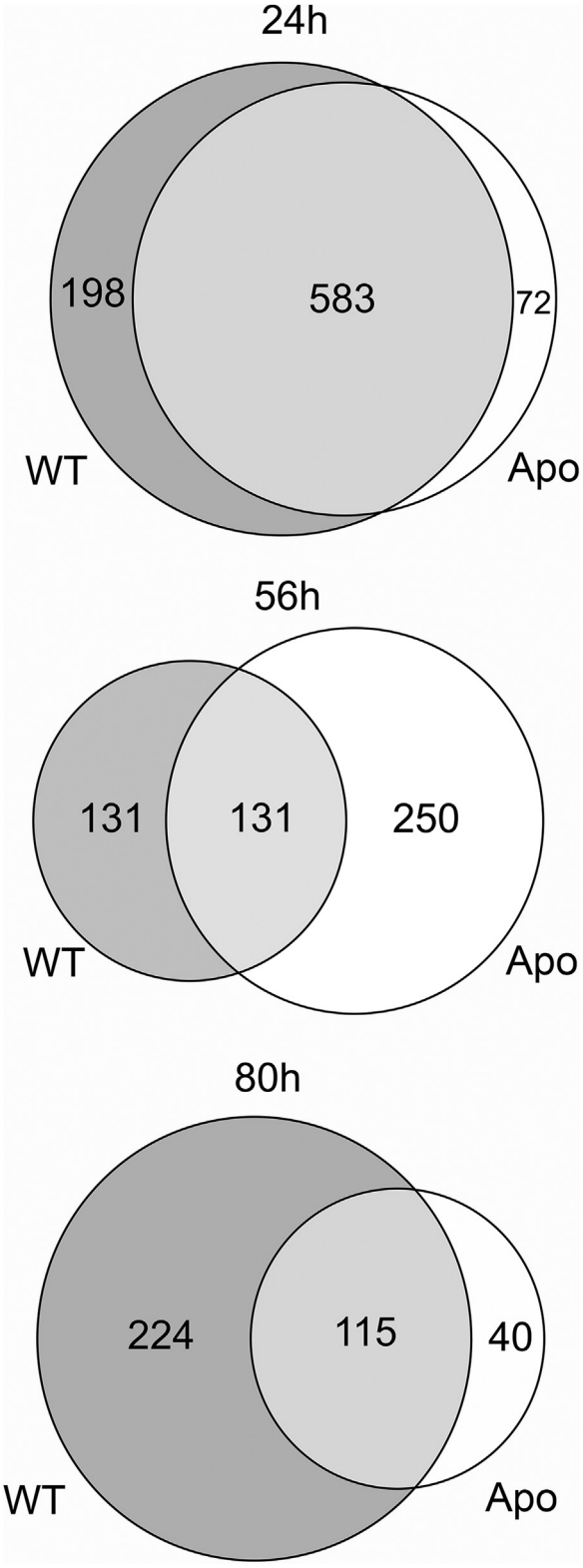

Figure 4. Area-proportional Venn diagrams showing the number of proteins that were identified at each time point. Diagrams were built inserting the numbers from PatternLab software directly into the RStudio. At the initial growth phase (**24 h**), a total of 655 proteins were identified for the aposymbiotic (Apo) strain, of which

Comparative Analysis of WT and Apo Strains at a Selected Time Point (56 h)

We have compared the proteins identified at each growth time point for all possible combinations between both strains. The WT 56 h x Apo 56 h combination presented the lowest overlap of identified proteins, which prompted us to further detail the analysis at this time point. Furthermore, the data from the comparisons for all other possible combinations did not bring additional original information. A detailed analysis of the 56 h time point revealed several dehydrogenases, transferases, synthases, tRNA synthetases for amino acid synthesis, ribosomal subunits components, elongation and initiation factors for protein synthesis, chaperones, and T-complex protein for protein folding were found exclusively or more abundant in the Apo strain (Supplementary Tables A.3c and A.5b). Among the ones found more abundant in the WT strain, mitochondrial electron transport chain proteins such as cytochrome c, cytochrome c oxidase subunit IV and subunit V, and F-type H+-transporting ATPase subunit delta were detected (Supplementary Tables A.3d and A.5b). On the other hand, peptidases (amino-, metallo-, and proteasome endopeptidases); enzymes of the above cited energy metabolism pathways (3,2-trans-enoyl-CoA isomerase, acyl-CoA dehydrogenase, glyceraldehyde-3-phosphate dehydrogenase, and pyruvate kinase), enzymes of the pentose phosphate pathway (glucose-6-phosphate 1-dehydrogenase, 6-phosphogluconate dehydrogenase, and transketolase), and typical mitochondrial proteins (aconitase and fumarate hydratase) were only found in the Apo strain. Distinct lipid catalytic proteins were found exclusively in each strain: enoyl reductase and myo-inositol-1-phosphate synthase were identified only in the Apo strain, while acyl carrier protein, phosphatidylserine decarboxylase, and lysosomal/endosomal membrane protein identified only in the WT strain (Supplementary Tables A.3c-d and A.5b). At 56 h, the enzymes coproporphyrinogen III oxidase and protoporphyrinogen oxidase, involved in heme biosynthesis, as well as detoxification enzymes nitroreductase, alcohol dehydrogenase, glutathione synthetase, iron superoxide dismutase, trypanothione synthetase-like protein, trypanothione-disulfide reductase, 3-hydroxyacyl-CoA dehydrogenase, tyrosine 3-monooxygenase/tryptophan 5-monooxygenase activation protein, thiol-dependent reductase 1, prostaglandin F synthase, and glutathione-S-transferase/glutaredoxin were exclusively found in Apo (Supplementary Table A.3c).

Abundance of Energy- and Carbohydrate-derived Metabolisms and Protein Biosynthesis-related Proteins Along the Growth Curve

Next, we focused on the identified proteins categorized in the two most represented ontologies: energy- and carbohydrate-derived metabolisms (glycolysis, electron transport chain, tricarboxylic acid cycle, and pentose pathway) and protein biosynthesis (ribosomal, tRNA-aminoacylation). The data were plotted as heatmaps according to the total number of spectra acquired at each time point (Figs 5, 6). Overall, the abundance of proteins in each categorization across the growth curve for each strain depicts a pattern. For instance, for both strains, the glycolytic proteins fructose bisphosphate aldolase class I, enolase, and glyceraldehyde 3-phosphate dehydrogenase displayed higher abundance at 24 h, with a reduction in the mid log phase (56 h). In the late log phase (80 h), the abundance of these three proteins was further reduced in the Apo strain, while in WT strain the proteins fructose bisphosphate aldolase class I and pyruvate dehydrogenase E1 beta increased their abundance by 67% (from 46 spectral counts at 56 h to 77 at 80 h) and 133% (from 21 spectral counts at 56 h to 49 at 80 h), respectively, compared to 56 h (Fig. 5A, B). Furthermore, Apo strain proteins from the biosynthetic pathway (small subunit ribosomal protein SAe, aspartate ammonia ligase, and glycyl-tRNA synthetase) presented their highest abundance at 24 h, with a gradual decrease over time until 80 h. On the other hand, for WT, these pro-

72 were only identified in this group. For the wild (WT) strain, a total of 781 proteins were identified, of which 198 were exclusively detected in this condition. At mid phase (**56 h**), 381 proteins were identified for Apo (250 exclusively detected), while 262 proteins were identified in WT (131 exclusively detected). Finally, at the late phase (**80 h**), from the 155 identified proteins in Apo, only 40 were exclusively detected in this condition while, for WT, 339 proteins (224 exclusively detected) were reported. The numbers for the overlays of the two strains at each time point (24 h, 56 h, and 80 h) are indicated in the diagram.

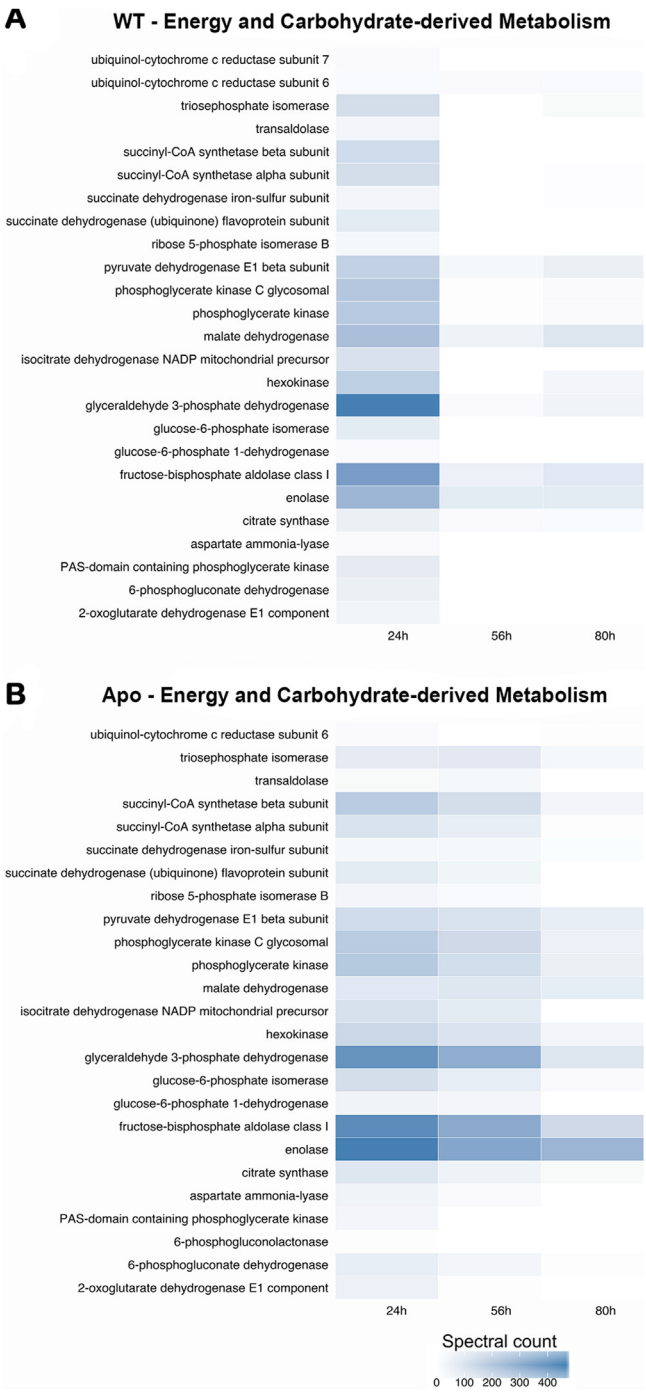

Figure 5. Quantitative heatmap of identified proteins, representatives of energy- and carbohydrate-derived metabolisms according to Gene Ontology, along the growth curve for (**A**) wild type (WT) and (**B**) aposymbiotic (Apo) strains. The scale bar is a gradient representation of the sum of the number of spectral counts of the replicates for each time point for each strain: White: no spectral count, 0. Dark blue: maximum number of spectra, 434 (For interpretation of the references to color in this figure legend, the reader is referred to the web version of this article).

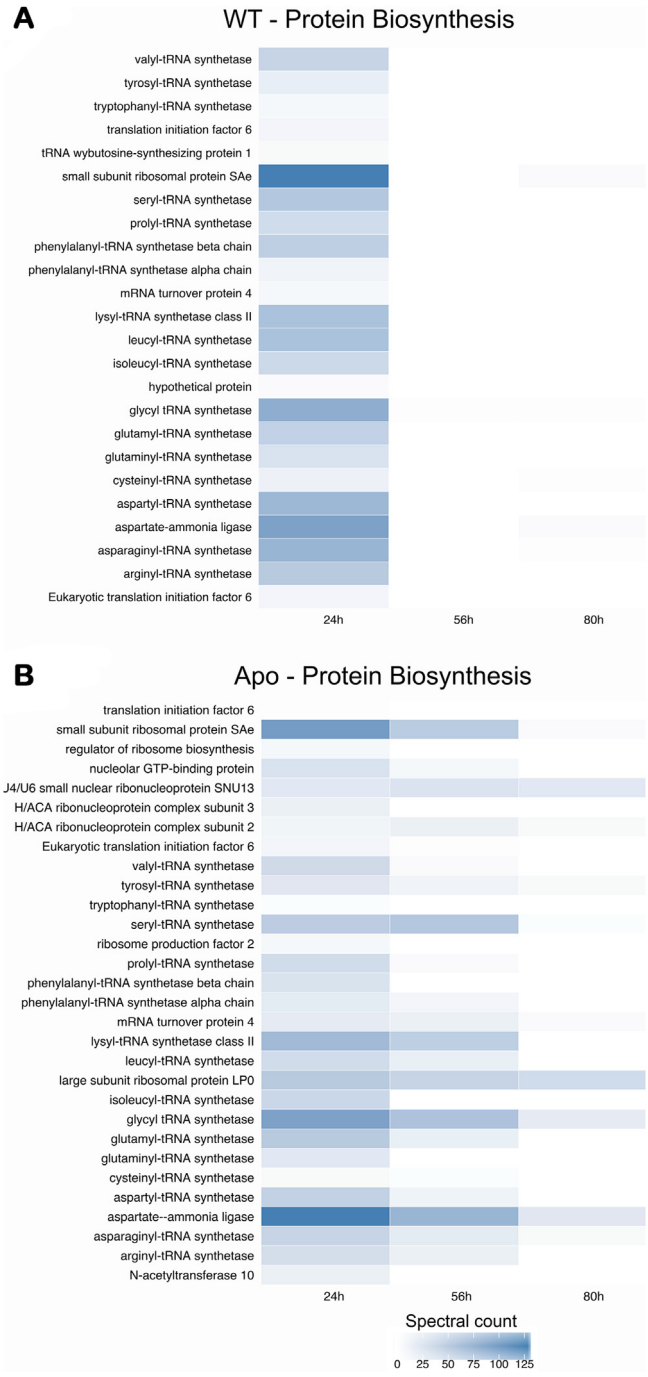

Figure 6. Quantitative heatmap of identified proteins, representatives of protein biosynthesis according to Gene Ontology, along the growth curve for (**A**) wild type (WT) and (**B**) aposymbiotic (Apo) strains. The scale bar is a gradient representation of the sum of the number of spectral counts of the replicates for each time point for each strain: White: no spectral count, 0. Dark blue: maximum number of spectra, 143 (For interpretation of the references to color in this figure legend, the reader is referred to the web version of this article).

Table 1. List of the differentially abundant proteins between aposymbiotic (Apo) and wild type (WT) strains at growth-curve time points 24 h, 56 h, and 80 h.

Accession number	Description	Growth-curve time point					
		24 h		56 h		80 h	
		Fold-change[a]	*p*-value	Fold-change[a]	*p*-value	Fold-change[a]	*p*-value
528204894	SC 4.3.1.1 aspartate ammonia-lyase	2.600	2.41E-03	NSD	NSD	NSD	NSD
528205547	SC large subunit ribosomal protein LP2	NSD[b]	NSD	NSD	NSD	−1.588	9.72E-03
528212366	SC mitotubule-associated protein Gb4	NSD	NSD	3.750	5.71E-04	NSD	NSD
528212431	SC RNA binding protein-like protein	−2.250	1.52E-02	NSD	NSD	NSD	NSD
528214344	SC cellular nucleic acid-binding protein	−1.625	2.78E-02	−5.067	1.97E-04	−4.267	2.46E-03
528214442	SC prostaglandin f synthase	2.333	2.67E-02	NSD	NSD	NSD	NSD
528214617	SC kinetoplastid membrane protein KMP-11	NSD	NSD	−2.889	9.23E-05	NSD	NSD
528214720	SC elongation factor 2	NSD	NSD	NSD	NSD	1.545	6.62E-03
528214843	SC small subunit ribosomal protein S24e	NSD	NSD	NSD	NSD	−2.200	6.62E-03
528215039	SC 1.4.4.2 glycine dehydrogenase	−2.889	4.95E-02	NSD	NSD	NSD	NSD
528215074	SC calmodulin	NSD	NSD	−4.000	1.00E-05	NSD	NSD
528215266	SC 1.1.1.37 malate dehydrogenase	NSD	NSD	4.167	3.43E-04	NSD	NSD
528215323	SC 1.1.99.2 2-hydroxyglutarate dehydrogenase	NSD	NSD	8.333	1.70E-03	NSD	NSD
528215528	SC translation initiation factor 5B	−4.000	3.27E-03	NSD	NSD	NSD	NSD
528215750	SC 2.7.9.1 pyruvate.orthophosphate dikinase	NSD	NSD	NSD	NSD	2.800	6.22E-03
528216304	SC 1.6.5.5 NADPH2:quinone reductase	3.778	2.63E-03	NSD	NSD	NSD	NSD
528217087	SC ATP-binding protein cassette. sub-family F. member 2	−1.632	1.12E-02	NSD	NSD	NSD	NSD
528217166	SC calreticulin	−1.923	6.62E-03	NSD	NSD	NSD	NSD
528217411	SC 3.6.3.14 ATP synthase beta chain. mitochondrial precursor	NSD	NSD	NSD	NSD	2.750	1.76E-02
528217459	SC pumilio like proteiny domain family member 6	−3.250	3.70E-02	NSD	NSD	NSD	NSD
528219961	SC translation initiation factor 5	−1.833	3.75E-03	NSD	NSD	NSD	NSD
528221636	SC 5.2.1.8 peptidylprolyl isomerase	−2.125	1.67E-02	NSD	NSD	NSD	NSD
528221880	SC cytochrome c oxidase subunit IV	NSD	NSD	−5.407	1.41E-03	NSD	NSD

Table 1 (*Continued*)

Accession number	Description	Growth-curve time point					
		24 h		56 h		80 h	
		Fold-change[a]	*p*-value	Fold-change[a]	*p*-value	Fold-change[a]	*p*-value
528221968	SC molecular chaperone GrpE	NSD	NSD	−5.556	3.43E-05	NSD	NSD
528222211	SC nascent polypeptide-associated complex subunit alpha	−1.625	1.21E-02	−6.143	1.00E-05	−4.083	2.13E-03
528222286	SC large subunit ribosomal protein LP0	−2.100	7.09E-03	NSD	NSD	NSD	NSD
528222653	SC proliferating cell nuclear antigen	−2.000	1.38E-02	NSD	NSD	NSD	NSD
528222811	SC 6.1.1.20 phenylalanyl-tRNA synthetase beta chain	−1.786	2.80E-02	NSD	NSD	NSD	NSD
528223515	SC 4.1.2.13 fructose-bisphosphate aldolase. class I	NSD	NSD	4.667	3.60E-04	NSD	NSD
528223697	SC molecular chaperone HtpG	NSD	NSD	NSD	NSD	3.000	8.07E-03
528224249	SC lipoprotein. type 6	NSD	NSD	−8.800	1.16E-03	NSD	NSD
528224543	SC heat shock 70 kDa protein 5	NSD	NSD	2.500	1.46E-05	NSD	NSD
528224769	SC 5.3.1.8 mannose-6-phosphate isomerase	−1.733	2.57E-02	NSD	NSD	NSD	NSD
528225178	SC small subunit ribosomal protein S3Ae	−1.452	1.10E-03	NSD	NSD	2.250	3.38E-03
528225947	SC flagellar associated protein	NSD	NSD	NSD	NSD	−3.000	5.37E-03
528226351	SC cytochrome c oxidase subunit V	−2.667	3.75E-03	−6.000	1.00E-05	NSD	NSD
528227180	SC stress-inducible protein STI1	−2.889	1.11E-02	NSD	NSD	NSD	NSD
528227814	SC cofilin	NSD	NSD	−2.600	7.86E-05	−1.846	2.43E-02
528227906	SC tyrosine 3-monooxygenase/tryptophan 5-monooxygenase activation protein	−1.625	5.53E-03	NSD	NSD	NSD	NSD
528228010	SC 1.6.5.5 oxidoreductase	1.773	2.89E-03	NSD	NSD	NSD	NSD
528228892	SC elongation factor 1-beta	−2.500	2.75E-02	5.333	1.01E-04	NSD	NSD
528229036	SC translation initiation factor 3 subunit E	−3.167	1.57E-02	NSD	NSD	NSD	NSD
528229166	SC 6.3.1.1 aspartate–ammonia ligase	NSD	NSD	NSD	NSD	3.667	4.23E-03
528229565	SC 2.3.1.12 pyruvate dehydrogenase E2 component (dihydrolipoamide acetyltransferase)	NSD	NSD	NSD	NSD	−2.000	2.12E-02
528229859	SC large subunit ribosomal protein L10Ae	−3.778	4.57E-03	NSD	NSD		
528229998	SC 2.7.4.6 nucleoside diphosphate kinase B	NSD	NSD	NSD	NSD	−1.400	2.37E-02

528230186	SC 1.11.1.- glutathione peroxidase-type tryparedoxin peroxidase	NSD	NSD	NSD	NSD	−2.533	2.47E-02
528230238	SC leucine rich repeat protein	−1.667	3.52E-02	NSD	NSD	NSD	NSD
528230629	SC large subunit ribosomal protein L22e	1.833	1.52E-02	NSD	NSD	NSD	NSD
528230669	SC large subunit ribosomal protein L37Ae	NSD	NSD	NSD	NSD	−2.750	3.88E-03
528232110	SC 1.1.1.205 IMP dehydrogenase	−2.200	6.62E-03	NSD	NSD	NSD	NSD
528232438	SC ribonucleoprotein p18. mitochondrial precursor	NSD	NSD	NSD	NSD	−6.714	1.00E-05
528232528	SC histone H2A	−2.000	4.77E-02	NSD	NSD	NSD	NSD
528233043	SC translation initiation factor 4A	NSD	NSD	13.000	1.58E-05	5.000	3.74E-02
528233943	SC aminopeptidase	−1.941	3.59E-03	NSD	NSD	NSD	NSD
528233969	SC translation initiation factor 5A	NSD	NSD	NSD	NSD	−3.238	5.76E-03
528234309	SC large subunit ribosomal protein L40e	NSD	NSD	−5.333	1.01E-04	NSD	NSD
528234311	SC large subunit ribosomal protein LP1	2.333	2.67E-02	−8.500	2.24E-04	NSD	NSD
528234523	SC syntaxin 6	2.333	2.67E-02	NSD	NSD	NSD	NSD
528234688	SC elongation factor 1-alpha	−1.689	2.97E-03	NSD	NSD	NSD	NSD
528234814	SC large subunit ribosomal protein L7Ae	NSD	NSD	NSD	NSD	1.929	2.51E-02
528235329	SC 5.4.2.8 phosphomannomutase	NSD	NSD	NSD	NSD	1.727	2.37E-02
528235542	SC 4.2.1.11 enolase	1.368	1.67E-03	NSD	NSD	NSD	NSD
528236382	SC 2.7.2.3 PAS-domain containing phosphoglycerate kinase	−1.923	2.18E-02	NSD	NSD	NSD	NSD
528236789	SC 2.1.1.- arginine N-methyltransferase	−2.133	2.84E-02	NSD	NSD	NSD	NSD
528238298	SC 1.1.1.22 UDPglucose 6-dehydrogenase	−2.000	2.94E-02	NSD	NSD	NSD	NSD
528238674	SC heat shock 70 kDa protein 1/8	NSD	NSD	NSD	NSD	−2.000	1.38E-02
528239463	SC large subunit ribosomal protein L36e	NSD	NSD	−2.083	1.01E-04	−2.800	7.90E-03
528239961	SC small subunit ribosomal protein S6e	NSD	NSD	NSD	NSD	1.875	3.65E-02
528240484	SC 1.10.2.2 ubiquinol-cytochrome c reductase iron-sulfur subunit	−2.000	3.88E-03	NSD	NSD	NSD	NSD
528242555	SC calpain-like cysteine peptidase	NSD	NSD	NSD	NSD	−2.077	1.24E-02
528242615	SC RNA-binding protein.. UPB1	NSD	NSD	−2.917	1.06E-05	NSD	NSD
528242968	SC elongation of very long chain fatty acids protein 4	1.714	3.75E-03	NSD	NSD	NSD	NSD
528243104	SC IgE-dependent histamine-releasing factor	NSD	NSD	−5.250	6.19E-05	−5.154	7.90E-04
528243740	SC cytochrome c	NSD	NSD	−3.857	2.81E-04	−4.111	1.10E-03
528244291	SC small subunit ribosomal protein S4e	NSD	NSD	NSD	NSD	2.143	2.67E-02

Table 1 (*Continued*)

Accession number	Description	Growth-curve time point					
		24 h		56 h		80 h	
		Fold-change[a]	*p*-value	Fold-change[a]	*p*-value	Fold-change[a]	*p*-value
528245036	SC large subunit ribosomal protein L10e	NSD	NSD	NSD	NSD	1.800	4.23E-03
528247111	SC kinetoplast DNA-associated protein	NSD	NSD	−3.583	5.06E-05	−3.867	1.34E-02
528247116	SC HSP20 family protein	NSD	NSD	−1.333	1.00E-05	NSD	NSD
528247266	SC 3.6.3.14 F-type H+-transporting ATPase subunit delta	NSD	NSD	−5.500	3.26E-04	−8.143	4.67E-05
528249060	SC solute carrier family 25 (mitochondrial carnitine/acylcarnitine transporter). member 20/29	1.556	3.75E-03	NSD	NSD	NSD	NSD
528249866	SC 3.4.11.18 metallo-peptidase. Clan MG. Family M24	1.769	4.45E-02	NSD	NSD	NSD	NSD
528250004	SC U4/U6 small nuclear ribonucleoprotein SNU13	NSD	NSD	NSD	NSD	−3.500	1.06E-03
528250651	SC 6.1.1.19 arginyl-tRNA synthetase	−2.889	2.45E-02	NSD	NSD	NSD	NSD
528250665	SC nuclear lim interactor-interacting factor-like protein	−2.400	1.24E-02	NSD	NSD	NSD	NSD
528250924	SC small subunit ribosomal protein S25e	NSD	NSD	−3.667	6.62E-04	NSD	NSD
528251062	SC solute carrier family 25 (mitochondrial adenine nucleotide translocator). member 4/5/6/31	−3.286	2.69E-02	NSD	NSD	NSD	NSD
528251409	SC 1.6.99.3 NADH dehydrogenase	2.091	1.63E-02	NSD	NSD	NSD	NSD
528251463	SC 1.8.1.4 dihydrolipoamide dehydrogenase	NSD	NSD	NSD	NSD	−2.250	2.88E-02
528252276	SC 5.2.1.8 peptidylprolyl isomerase	NSD	NSD	−6.000	1.28E-04	NSD	NSD
528252603	SC nascent polypeptide-associated complex subunit beta	NSD	NSD	NSD	NSD	−2.375	2.80E-02
528253965	SC 2.6.1.5 tyrosine aminotransferase	1.667	3.52E-02	NSD	NSD	NSD	NSD
528254677	SC 4.2.1.46 dTDP-glucose 4.6-dehydratase	−2.500	3.01E-02	NSD	NSD	NSD	NSD
528256028	SC 6.2.1.3 fatty acyl CoA synthetase 2	−1.857	6.62E-03	NSD	NSD	NSD	NSD
528257416	SC 6.1.1.4 leucyl-tRNA synthetase	−1.938	2.12E-02	NSD	NSD	NSD	NSD
528257524	SC small subunit ribosomal protein S12e	NSD	NSD	NSD	NSD	−3.400	1.12E-02
528257664	SC kinesin K39	NSD	NSD	−4.650	9.77E-05	−6.167	2.21E-04

[a]Positive fold-change values reflect higher abundance in the aposymbiotic strain while negative fold-change values reflect higher abundance in the wild-type strain.
[b]NSD - No statiscally significant difference.

teins were only detected, albeit abundantly, at 24 h (Fig. 6A, B).

Discussion

Endosymbiosis in trypanosomatids was first reported in 1907 (Novy et al. 1907), but only in 1963 the bacterial presence was confirmed (Marmur et al. 1963). Since then, several advances in microscopy, biochemistry, as well as RNA and DNA sequencing methods have allowed a detailed characterization of the intricated interaction between trypanosomatids and their bacterial symbiont (Alves et al. 2013b; Bombaça et al. 2017; Loyola-Machado et al. 2017; Motta et al. 2010; Motta et al. 2013; Penha et al. 2016). For instance, the involvement of the symbiont in different metabolic pathways, such as vitamins, amino acid and heme biosyntheses, was demonstrated initially through classical biochemical approaches (Camargo and Freymuller 1977; Chang et al. 1975; Galinari and Camargo 1978; Salzman et al. 1985) and was recently inferred by whole genome sequencing (Alves et al. 2011, 2013a; Klein et al. 2013). Since trypanosomatids (including *S. culicis*) present post-transcriptional gene regulation, proteomics is an attractive approach to monitor and confirm protein expression in these protists (Brunoro et al. 2015; Clayton and Shapira 2007; Parodi-Talice et al. 2004).

In this study, mass spectrometry-based proteomics was employed to generate the first quantitative differential proteomic data on the symbiont-harboring trypanosomatid *S. culicis*, in the presence (WT) or absence (Apo) of its bacterial symbiont, along a growth curve timeline. The time point at 56 h was selected for a more detailed data analysis since it presented the lowest overlap of protein identifications between both strains.

The endosymbiotic bacterium contributes to the protist metabolism providing enzymes (absent in the host) for essential routes such as amino acid (especially ornithine and lysine), vitamin (riboflavin), and heme biosynthesis (Alves et al. 2011, 2013a; Chang et al. 1975; Klein et al. 2013). Concurring with these previous observations, our proteomic approach showed that, after elimination of the symbiont, the most affected biological processes were amino acid and protein syntheses and protein folding. For the Apo strain, an increase in the abundance of many proteins related to different steps of distinct amino acids biosynthesis was detected. For example, the well-known enzymes of the ornithine metabolism such as arginase, argininosuccinate synthase, and ornithine cyclodeaminase were more abundant in Apo strain, presumably in order to fulfill the absence of crucial enzymes to ornithine biosynthesis, provided by the bacterium, as previously demonstrated (Camargo and Freymuller 1977; Galinari and Camargo 1978).

As expected, the kinetic analysis showed that structural proteins related to cytoskeleton and motility, as well as proteins involved in gene expression regulation (histones, ribosomal components, elongation factors etc.), are expressed constitutively during the parasite growth in both strains. At all time points studied, WT and Apo also expressed proteins involved in bioenergetics (enolase, pyruvate dehydrogenase, among others) and antioxidant defenses (tryparedoxin peroxidase), important pathways to parasite proliferation and detoxification, respectively. It is worth noting that the total protein number identified at the initial time point analyzed [24 h – WT (781 proteins); Apo (655 proteins)] was higher than at 56 h [WT (262); Apo (381)] and 80 h [WT (339); Apo (155)], for both strains. The reasons for that are still unknown, but one possible contribution would be a higher frequency of post-translational modifications as the growth proceeded; this would not be detected by the peptide/protein identification approach used in this work, and could diminish the number of identifiable peptides/proteins. Even though the total number of proteins was highest at 24 h, both for WT and Apo strains, their distribution in essential biological processes (structural proteins, gene expression regulation, bioenergetic, and antioxidative pathways) prevailed up to 80 h. However, different endopeptidases and proteins related to amino acid and protein biosyntheses were also detected in both strains only at the early log phase (24 h), suggestive of an intense protein anabolism at the beginning of the proliferation curve.

Our proteomic analysis revealed enzymes involved in the synthesis of several amino acids such as cysteine, glutamine, threonine, tyrosine, serine, methionine, homoserine, glutamate, alanine, asparagine, arginine, and valine in the symbiont-free strain, pointing to the occurrence of a compensatory mechanism to ensure that Apo cells will have at least the minimum levels of these amino acids to survive. Besides, our data also reinforce the participation of the symbiont in amino acid and protein syntheses (Alves et al. 2013a; Novak et al. 1988). Accordingly, it has been previously demonstrated that the Apo strain secretes more peptidases, probably reflecting a compensatory mechanism to obtain amino acids from the

culture media (D'Avila-Levy et al. 2005a). Regarding heme biosynthesis, the endosymbiont provides 7 out of a total of 11 enzymes involved in the production of this ferriprotoporphyrin-IX (Alves et al., 2011). The enzymes coproporphyrinogen III oxidase and protoporphyrinogen oxidase, involved in steps that take place in the protist cytosol (independently of bacterial presence), were also found in Apo cells, also suggesting an attempt to balance the elimination of the symbiont. In all trypanosomatids, the mitochondrion is a single organelle, remarkably branched, that concentrates the mitochondrial DNA network in a kinetoplast, as recently illustrated by three-dimensional reconstruction in *S. culicis* (Loyola-Machado et al. 2017). As in higher eukaryotes, mitochondrion plays a central role in energy transduction, which is totally dependent on complex II activity (de Souza et al. 2009; Liu et al. 2005). It was demonstrated first in *Angomonas deanei* that the symbiont enhances the host oxygen consumption and has respiratory capacity once isolated from the protist (Azevedo-Martins et al. 2015). Later on, biochemical analysis of *S. culicis* pointed to metabolic differences between the mitochondrion of WT and Apo cells, indicating an uncoupled profile of the organelle in the protist without the symbiont (Bombaça et al. 2017; Loyola-Machado et al. 2017). The Apo cell shotgun proteomics results, reported herein, revealed many enzymes associated to different pathways that culminate in ATP production. Some enzymes from pentose phosphate pathway, glycolysis, as well as from typical mitochondrial metabolism, such as steps of tricarboxylic acid cycle, were all present after the elimination of the symbiont, once more suggesting a metabolic regulation to compensate for the absence of the bacterium. Global time course evaluation of WT cells presented a higher abundance of proteins related to energy metabolism and pentose phosphate pathway only in 24 h, while more abundant proteins involved in this biological process could be detected at all time points analyzed for the Apo strain. Interestingly, three well-known enzymes of the glycolytic pathway were remarkably abundant during Apo cell cycle: enolase, fructose-bisphosphate aldolase, and glyceraldehyde 3-phosphate dehydrogenase, reinforcing the fermentative behavior of this strain (Loyola-Machado et al. 2017).

In relation to the mitochondrial electron transport system (ETS), WT presented higher abundance of complexes III, IV and cytochrome c (up to 6-fold in the case of cytochrome c oxidase), while complexes I, II, and ATP synthase were present in higher amounts in the Apo strain. The increase in the expression of initial steps of oxidative phosphorylation detected in Apo is in accordance with previous analyses of the mitochondrial functionality for both strains. Such analyses demonstrated differences in the oxidative phosphorylation of WT and Apo strains, showing an uncoupled ETS for the strain without the symbiont. Again, one possible interpretation is that the increase in abundance for complexes I and II could represent a compensatory mechanism in response to the low ATP levels, derived from low oxidative phosphorylation activity in the Apo strain (Bombaça and Menna-Barreto 2017; Galvez Rojas et al. 2008).

S. culicis and other trypanosomatids are frequently challenged by reactive oxygen species (ROS) in their different hosts. Hence, the adaptation of these protists to environmental conditions is mandatory for their survival (Bombaça and Menna-Barreto 2017). Based on biochemical approaches, our group has previously demonstrated that the Apo strain presents impaired mitochondrial function and produces high levels of hydrogen peroxide in comparison to WT cells (Bombaça et al. 2017). The data from the present work pointed to the identification of many enzymes associated with detoxification processes (ammonia, alcohol, nitric oxide, and ROS scavengers) in Apo strain, reinforcing our previous data showing the increased ROS generation in the absence of the symbiont, and supporting the hypothesis of the bacterial role in oxidative conditions. Additionally, an increase in pentose phosphate pathway was also detected in Apo strain. This pathway has an important role to generate NADPH as source of reducing power, taking particular importance to parasite survival into pro-oxidant environment (Kovarova and Barrett 2016). The increased expression of proteins related to oxidative branch (glucose-6-phosphate 1-dehydrogenase and 6-phosphogluconate dehydrogenase) can be related to high ROS concentrations previously described in aposymbiotic strain (Bombaça et al. 2017) and supports the hypothesis that the symbiont elimination impairs the protist antioxidant system.

Among the identified proteins related to fatty acid catabolism and biosynthesis, almost all were present in Apo cells too, suggesting alterations in biological membrane composition and dynamics. The detection, in WT cells only, of phosphatidylserine decarboxylase - an enzyme responsible for the phosphatidylserine synthesis – is in line with reported differences in lipid content between both strains and reinforces the notion that the symbiont influences phospholipid anabolism in the host trypanosomatid (Azevedo-Martins et al. 2007, 2015).

Efforts must be made in this direction to propose the biological impact (if any) of these findings.

The protist surface plays a primary role in response to extracellular events. In this context, the plasma membrane composition, in special glycoconjugates, is fundamental for specific recognition, triggering several biological processes (D'Avila-Levy et al. 2005a, b). Among the glycoconjugates present in trypanosomatids surface, glycoproteins and glycolipids are the most abundant. Previous data from our group pointed to the crucial importance of *S. culicis* surface saccharides for the adhesion to the midgut of the invertebrate host (D'Avila-Levy et al. 2005b). The pre-incubation of parasites with mucin, fetuin, and sialyllactose, as well as mannose-rich molecules, led to a remarkable reduction of the binding of this trypanosomatid to the epithelial cells of the insect's intestine. Here, our data showed the presence in the Apo strain of a mucin-associated surface protein and a mannose-6-phosphate isomerase. Such isomerase is an enzyme that participates in GDP-mannose biosynthesis, one of the most common surface glycoconjugates in trypanosomatids (Turnock and Ferguson 2007). Differences in the surface composition between the two strains can sum up to the possible explanation of the better interaction of the endosymbiont-containing cells with the host cells, as previously demonstrated (D'Avila-Levy et al. 2005b; Fampa et al. 2003). In addition, an impaired ability to colonize the insect host is well reported for the Apo strain (Bombaça et al. 2017; Corrêa-da-Silva et al. 2006). Several parasite proteins play a concerted action in this process and the molecular interactions that take place in the insect midgut are unpredictable. Although the individual role of enzymes in this interaction has been demonstrated (Catta-Preta et al. 2013; D'Avila-Levy et al. 2005a, 2008), this kind of information is still insufficient to fully elucidate the functional impact of the complex structures that could be formed and the influence of the microenvironment of the insect midgut on such structures. A glycomic/glycoproteomic analysis of both strains should help understanding the interaction of the endosymbiont-containing cells with the host cells, although this was not within the scope of the present work.

Conclusion

This work provided new data on the contribution of the endosymbiont to different metabolic pathways of *S. culicis* and analyzed, for the first time, the overall protein expression in this trypanosomatid, while performing a side-by-side comparison of protein abundance between the wild type and the aposymbiotic strains. These data represent a promising starting point for the selection of key proteins to be further explored to help understanding the interactions between monoxenous trypanosomatids and invertebrate hosts, as well as the biology of endosymbiont-bearing trypanosomatids.

Methods

Trypanosomatids cultures: *S. culicis* WT and Apo strains - COLPROT041 and COLPROT034, respectively - were provided by Fiocruz Protist Collection (http://colprot.fiocruz.br) and grown at 28 °C in a medium devised to sustain glycolytic growth (LIT - liver infusion 5.0 g/L, tryptose 5.0 g/L, NaCl 4.0 g/L, KCl 0.4 g/L, $Na_2HPO_4.H_2O$ 4.3 g/L, glucose D+2.0 g/L) supplemented with 20% heat-inactivated fetal bovine serum (Sigma) and 0.1% hemin. To define the growth phases for each strain, the cultures were inoculated with parasites collected at the log phase to a final density of 1×10^6 cells/mL. At different time points, three aliquots from the total cellular culture (100 μL) were collected and quantified in a Neubauer chamber. This experiment was performed in triplicate (inocula from three independent cultures).

DNA extraction, PCR amplification, sequencing, and phylogenetic analyses: Total DNA from at least 5×10^6 cells was extracted from cultured trypanosomatids at mid-log growing phase using the Wizard® Genomic DNA purification kit according to manufacturer's protocol (Promega, Madison, USA). The partial sequence of the gGAPDH gene was PCR-amplified using previously described primers and PCR conditions (Teixeira et al. 2011). The amplified DNA segments were sequenced directly as described previously (Ishemgulova et al. 2017). The sequences were deposited under the following GenBank accession numbers: KX901487 (COLPROT034) and KX901488 (COLPROT041). gGAPDH sequences were aligned using multiple sequence alignment with high accuracy and high throughput (MAFFT) online server and manually refined in BioEdit (Hall 1999). Bayesian tree was reconstructed in MrBayes v3.2. (Huelsenbeck et al. 2001), using GTR + I+G as substitution model, selected in JModelTest according to Akaike criterion (Posada 2008), with 5,000,000 generations with trees sampled every 10,000 generations using chains, and 25% of the early sample trees were discarded. Other parameters of MCMC were set as default (Ronquist et al. 2012).

Transmission electron microscopy (TEM) analysis: Epimastigotes of both strains (5.0×10^7 parasites/mL) were washed with phosphate buffered saline (PBS, pH 7.2) and fixed with 2.5 % glutaraldehyde diluted in 0.1 M sodium cacodylate buffer (pH 7.2) for 30 min and subsequently postfixed in a solution of 1% OsO4 containing 0.8 % potassium ferricyanide and 2.5 mM calcium chloride in the same buffer for 20 min. The dehydration steps were performed in an ascending acetone series and the cells were embedded in PolyBed 812 resin. Ultrathin sections were obtained, stained with uranyl acetate and lead citrate, and then examined in a transmission electron microscope JEM 1011 (Jeol, Tokyo, Japan) at Plataforma de Microscopia Eletrônica, Fiocruz.

Sample preparation for mass spectrometry analysis: For each strain (WT or Apo), three independent biological replicates were processed at different times of growth (24 h,

56 h, and 80 h). At each time point, parasites were quantified in a Neubauer chamber. Parasites (1×10^8 cells) were initially washed three times by successive cycles of phosphate buffered saline (pH 7.4) addition, centrifugation at 3,000 *g* for 10 min, and supernatant disposal. Washed parasites were incubated with 100 μL of 0.25% (w/v) Rapigest SF surfactant (Waters Corporation, MA, USA) in 50 mM ammonium bicarbonate. Subsequently, 5 freeze-thaw cycles with liquid nitrogen were performed, followed by 5 min in boiling water, 5 min on ice, and centrifugation at 14,000 *g* for 10 min. The supernatants containing the protein lysates were collected and quantified by the bicinchoninic acid protein assay (Merck, Damstadt, GE). Fifty micrograms per sample were further processed by the addition of dithiotreitol to a final 20 mM concentration and heated for 30 min at 60 °C, followed by cooling to room temperature, addition of iodoacetamide (67 mM final concentration), and incubation for 15 min (in the dark) at room temperature. Porcine trypsin (V511, Promega Corporation, Madison, USA) was added at 1:50 (m/m) enzyme to substrate ratio and incubation proceeded for 16 h at 37 °C, followed by 45 min at 56 °C. Reaction was stopped by addition of trifluoroacetic acid to a 0.5% (v/v) final concentration and incubation for 45 min at 37 °C. Samples were centrifuged at 16,000 *g* for 10 min and supernatants were subjected to reversed-phase desalting with Poros R2 matrix homemade tip-columns, followed by dryness to completion, and storage at -20 °C until use, as described elsewhere (Caminha et al. 2019).

Reversed-phase chromatography online with mass spectrometry: Desalted tryptic digests, prepared as described in the previous step, were each resuspended in 30 μL of 1% (v/v) formic acid. Each sample was analyzed in technical triplicate on an EASY-nLC-System (Proxeon Biosystems, West Palm Beach, USA) hyphenated to an LTQ-Orbitrap XL mass spectrometer via a nanoscale LC interface (Thermo, USA). Chromatographic conditions and mass spectrometry settings were the same as previously described (Brunoro et al. 2015), although we have used a 30-cm long reversed-phase column and a different elution gradient (2 to 40% mobile phase B in 162 min).

Data analysis: The RAW data of the technical triplicate for each biological replicate were analyzed in the computer environment PatternLab for Proteomics (version 4.0, http://patternlabforproteomics.org) (Carvalho et al., 2016). Peptide-spectrum matching (PSM) was done using the Comet search engine (version 2016.01) against a database containing: a) *gi* numbered protein sequences from *Strigomonas culicis*, *Ca.* Kinetoplastibacterium blastocrithidii, and *Ca.* K. crithidii - derived from the literature (Motta et al. 2013) - and/or from the PubMed NCBI-hosted website (https://www.ncbi.nlm.nih.gov/protein/); b) reversed decoy entries for each protein sequence; c) 127 common protein contaminants sequences – total database number of entries of 19,452. For the Comet search, used parameters were: tryptic (allowing semi-tryptic) peptide candidates with masses between 550 and 5,500 Da; peptide sequences with up to two missed cleavages; 20 ppm for precursor mass and bins of 1.0005 m/z for MS/MS; methionine oxidation, and asparagine and glutamine deamidations as variable modifications, and carbamidomethyl cysteine as fixed modification. The mass spectrometry proteomics data have been deposited to the ProteomeXchange Consortium (http://proteomecentral.proteomexchange.org) via the PRIDE partner repository (Perez-Riverol et al. 2019) receiving the dataset identifier PXD013136. The validity of the PSM was assessed using the Search Engine Processor (SEPro) (Carvalho et al. 2012a). For each PSM, the XCorr, DeltaCN, and Spectral Count score values were used to generate a Bayesian discriminator. The spectra were filtered in 3 levels: first, 3% of decoys were accepted; secondly, the spectra were grouped according to their respective identified peptide sequences, converging to a classification that accepted only 2% of decoy peptides and 1% of decoy proteins (for a peptide to be considered identified, a minimum sequence length of 6 amino acid residues was required) and, finally, by applying post-processing filters, only identifications with < 10 ppm error and proteins with at least one peptide spectrum match with XCorr > 2.5 or two or more peptide spectrum matches with XCorr > 2.0 were accepted. Spectral count approach was used for the quantitative comparison in the TFold module of PatternLab for Proteomics, and only proteins for which the comparison reached a Benjamini–Hochberg q-value of 0.05 and presented a minimum of 8 spectra in one replicate per condition (L-stringency) were reported (Carvalho et al. 2012b). The fold–change cutoff of a protein was proportional to an exponential function of its *t*-test *p*-value as described in (Carvalho et al. 2012b). To build the exponent of this function an *F*-stringency value for each comparison was set ("Read me" tab of Supplementary Table A.5). For qualitative analysis, for each time point, a Venn diagram was built with PatternLab considering only the identifications present at least in 2 replicates per group (strain). The spectral count data exported from Project Organization tool of PatternLab For Proteomics was used for the heatmaps graphical representation. For both strains, the spectral counts of the biological replicates were summed for each protein and time point. For the functional description of the identified and quantified proteins, the Uniprot resource for protein sequence and annotation data was used. First, the NCBI identifiers of the proteins here described were converted to Uniprot identifiers (https://www.uniprot.org/). Then, the results were customized selecting the Gene Ontology biological process, molecular function, and cellular component columns. The annotation data were finally exported. After Gene Ontology analysis, the spectral count information of the proteins from glycolysis, electron transport chain, tricarboxylic acid cycle, ribosomal, tRNA-aminoacylation, and pentose pathway ontologies was selected for heatmaps construction in RStudio (Version 1.1.456).

Declaration of Interest

The authors declare no conflict of interest.

Acknowledgements

The present study was supported by Fundação Carlos Chagas Filho de Amparo à Pesquisa do Estado do Rio de Janeiro (FAPERJ), Brazil (E-26/111.781/2012 to R.H.V.). A.S.G.-G. was enrolled at the Cellular and Molecular Biology Graduate Program (FIOCRUZ, RJ, Brazil) as a fellow from the Conselho Nacional de Desenvolvimento Científico e Tecnológico, Brazil. At the time this manuscript was drafted, G.V.F.B. was the recipient of a post-doctoral fellowship from FAPERJ (E-26/202.739/2016).

Appendix A. Supplementary Data

Supplementary material related to this article can be found, in the online version, at doi:https://doi.org/10.1016/j.protis.2019.125698.

References

Alfieri SC, Camargo EP (1982) Trypanosomatidae: isoleucine requirement and threonine deaminase in species with and without endosymbionts. Exp Parasitol **53**:371–380

Alves JMP, Klein CC, da Silva F, Costa-Martins AG, Serrano MG, Buck GA, Vasconcelos ATR, Sagot M-F, Teixeira MMG, Motta MCM, Camargo EP (2013a) Endosymbiosis in trypanosomatids: The genomic cooperation between bacterium and host in the synthesis of essential amino acids is heavily influenced by multiple horizontal gene transfers. BMC Evol Biol **13**:190

Alves JMP, Serrano MG, Maia da Silva F, Voegtly LJ, Matveyev AV, Teixeira MMG, Camargo EP, Buck GA (2013b) Genome evolution and phylogenomic analysis of *Candidatus* Kinetoplastibacterium, the betaproteobacterial endosymbionts of *Strigomonas* and *Angomonas*. Genome Biol Evol **5**:338–350

Alves JMP, Voegtly L, Matveyev AV, Lara AM, da Silva FM, Serrano MG, Buck GA, Teixeira MMG, Camargo EP (2011) Identification and phylogenetic analysis of heme synthesis genes in trypanosomatids and their bacterial endosymbionts. PLoS One **6**:e23518

Azevedo-Martins AC, Frossard ML, de Souza W, Einicker-Lamas M, Motta MCM (2007) Phosphatidylcholine synthesis in *Crithidia deanei*: The influence of the endosymbiont. FEMS Microbiol Lett **275**:229–236

Azevedo-Martins AC, Machado ACL, Klein CC, Ciapina L, Gonzaga L, Vasconcelos ATR, Sagot MF, De Souza W, Einicker-Lamas M, Galina A, Motta MCM (2015) Mitochondrial respiration and genomic analysis provide insight into the influence of the symbiotic bacterium on host trypanosomatid oxygen consumption. Parasitology **142**:352–362

Bombaça ACS, Menna-Barreto RFS (2017) The Oxidative Metabolism in Trypanosomatids: Implications for These Protozoa Biology and Perspectives for Drugs Development. In Leon L, Torres-Santos EC (eds) Different Aspects on Chemotherapy of Trypanosomatids. Nova Science Publishers, e-book, pp 93–129

Bombaça ACS, Dias FA, Ennes-Vidal V, Garcia-Gomes AS, Sorgine MHF, d'Avila-Levy CM, Menna-Barreto RFS (2017) Hydrogen peroxide resistance in *Strigomonas culicis*: Effects on mitochondrial functionality and *Aedes aegypti* interaction. Free Radic Biol Med **113**:255–266

Brum FL, Catta-Preta CMC, de Souza W, Schenkman S, Elias MC, Motta MCM (2014) Structural characterization of the cell division cycle in *Strigomonas culicis*, an endosymbiont-bearing trypanosomatid. Microsc Microanal **20**:228–237

Brunoro GVF, Caminha MA, Ferreira ATS, Leprevost FV, Carvalho PC, Perales J, Valente RH, Menna-Barreto RFS (2015) Reevaluating the *Trypanosoma cruzi* proteomic map: The shotgun description of bloodstream trypomastigotes. J Proteomics **115**:58–65

Camargo EP, Freymuller E (1977) Endosymbiont as supplier of ornithine carbamoyltransferase in a trypanosomatid. Nature **270**:52–53

Caminha MA, Lorena VMB, Oliveira Júnior W, Perales J, Carvalho PC, Lima DB, Cavalcanti Md GAM, Martins SM, Valente RH, Menna-Barreto RFS (2019) *Trypanosoma cruzi* immunoproteome: Calpain-like CAP5. 5 differentially detected throughout distinct stages of human Chagas disease cardiomyopathy. J Proteomics **194**:179–190

Carvalho PC, Yates JR 3rd, Barbosa VC (2012b) Improving the TFold test for differential shotgun proteomics. Bioinformatics **28**:1652–1654

Carvalho PC, Fischer JSG, Xu T, Cociorva D, Balbuena TS, Valente RH, Perales J, Yates JR, Barbosa VC (2012a) Search engine processor: Filtering and organizing peptide spectrum matches. Proteomics **12**:944–949

Carvalho PC, Lima DB, Leprevost FV, Santos MDM, Fischer JSG, Aquino PF, Moresco JJ, Yates JR, Barbosa VC (2016) Integrated analysis of shotgun proteomic data with PatternLab for proteomics 4. 0. Nature Protoc **11**:102–117

Catta-Preta CMC, Nascimento MTC, Garcia MCF, Saraiva EM, Motta MCM, Meyer-Fernandes JR (2013) The presence of a symbiotic bacterium in *Strigomonas culicis* is related to differential ecto-phosphatase activity and influences the mosquito–protozoa interaction. Int J Parasitol **43**:571–577

Catta-Preta CMC, Brum FL, da Silva CC, Zuma AA, Elias MC, de Souza W, Schenkman S, Motta MCM (2015) Endosymbiosis in trypanosomatid protozoa: the bacterium division is controlled during the host cell cycle. Front Microbiol **6**:520

Chang KP, Trager W (1974) Nutritional significance of symbiotic bacteria in two species of hemoflagellates. Science **183**:531–532

Chang KP, Chang CS, Sassa S (1975) Heme biosynthesis in bacterium-protozoon symbioses: Enzymic defects in host hemoflagellates and complemental role of their intracellular symbiotes. Proc Natl Acad Sci USA **72**:2979–2983

Clayton C, Shapira M (2007) Post-transcriptional regulation of gene expression in trypanosomes and leishmanias. Mol Biochem Parasitol **156**:93–101

Corrêa-da-Silva MS, Fampa P, Lessa LP, Silva ER, Mallet JRS, Saraiva EMB, Motta MCM (2006) Colonization of *Aedes aegypti* midgut by the endosymbiont-bearing trypanosomatid *Blastocrithidia culicis*. Parasitol Res **99**:384–391

D'Avila-Levy CM, Araújo FM, Vermelho AB, Soares RMA, Santos ALS, Branquinha MH (2005a) Proteolytic expression in *Blastocrithidia culicis*: influence of the endosymbiont and similarities with virulence factors of pathogenic trypanosomatids. Parasitology **130**:413–420

D'Avila-Levy CM, Santos LO, Marinho FA, Matteoli FP, Lopes AHCS, Motta MCM, Santos ALS, Branquinha MH (2008) *Crithidia deanei*: Influence of parasite gp63 homologue on the interaction of endosymbiont-harboring and aposymbiotic strains with *Aedes aegypti* midgut. Exp Parasitol **118**:345–353

D'Avila-Levy CM, Silva BA, Hayashi EA, Vermelho AB, Alviano CS, Saraiva EMB, Branquinha MH, Santos ALS (2005b) Influence of the endosymbiont of *Blastocrithidia culicis* and *Crithidia deanei* on the glycoconjugate expression and on *Aedes aegypti* interaction. FEMS Microbiol Lett **252**:279–286

D'Avila-Levy CM, Boucinha C, Kostygov A, Santos HLC, Morelli KA, Grybchuk-Ieremenko A, Duval L, Votýpka J, Yurchenko V, Grellier P, Lukeš J (2015) Exploring the environmental diversity of kinetoplastid flagellates in the high-throughput DNA sequencing era. Mem Inst Oswaldo Cruz **110**:956–965

de Oliveira SSC, Garcia-Gomes AS, d'Avila-Levy CM, dos Santos ALS, Branquinha MH (2015) Expression of calpain-like proteins and effects of calpain inhibitors on the growth rate of *Angomonas deanei* wild type and aposymbiotic strains. BMC Microbiol **15**:188

de Souza W, Attias M, Rodrigues JCF (2009) Particularities of mitochondrial structure in parasitic protists (Apicomplexa and Kinetoplastida). Int J Biochem Cell Biol **41**:2069–2080

de Souza W, Motta MC (1999) Endosymbiosis in protozoa of the Trypanosomatidae family. FEMS Microbiol Lett **173**:1–8

Dwyer DM, Chang KP (1976) Surface membrane carbohydrate alterations of a flagellated protozoan mediated by bacterial endosymbiotes. Proc Natl Acad Sci USA **73**:852–856

Esteves MJ, Andrade AF, Angluster J, de Souza W, Mundim MH, Roitman I, Perreira ME (1982) Cell surface carbohydrates in *Crithidia deanei*: Influence of the endosymbiote. Eur J Cell Biol **26**:244–248

Fampa P, Corrêa-da-Silva MS, Lima DC, Oliveira SMP, Motta MCM, Saraiva EMB (2003) Interaction of insect trypanosomatids with mosquitoes, sand fly and the respective insect cell lines. Int J Parasitol **33**:1019–1026

Freymuller E, Camargo EP (1981) Ultrastructural differences between species of trypanosomatids with and without endosymbionts. J Protozool **28**:175–182

Gadelha C, Wickstead B, de Souza W, Gull K, Cunha-e-Silva N (2005) Cryptic paraflagellar rod in endosymbiont-containing kinetoplastid protozoa. Eukaryot Cell **4**:516–525

Galinari S, Camargo EP (1978) Trypanosomatid protozoa: survey of acetylornithinase and ornithine acetyltransferase. Exp Parasitol **46**:277–282

Galvez Rojas RL, Frossard ML, Machado Motta MC, Silber AM (2008) L-Proline uptake in *Crithidia deanei* is influenced by its endosymbiont bacterium. FEMS Microbiol Lett **283**:15–22

Hall TA (1999) BioEdit: a user-friendly biological sequence alignment editor and analysis program for Windows 95/98/NT. Nucleic Acids Symp Ser **41**:95–99

Harmer J, Yurchenko V, Nenarokova A, Lukes J, Ginger ML (2018) Farming, slaving and enslavement: histories of endosymbioses during kinetoplastid evolution. Parasitology **145**:1311–1323

Huelsenbeck JP, Ronquist F, Nielsen R, Bollback JP (2001) Bayesian inference of phylogeny and its impact on evolutionary biology. Science **294**:2310–2314

Ishemgulova A, Butenko A, Kortisova L, Boucinha C, Grybchuk-Ieremenko A, Morelli KA, Tesarova M, Kraeva N, Grybchuk D, Panek T, Flegontov P, Lukes J, Votypka J, Pavan MG, Opperdoes FR, Spodareva V, d'Avila-Levy CM, Kostygov AY, Yurchenko V (2017) Molecular mechanisms of thermal resistance of the insect trypanosomatid *Crithidia thermophila*. PLoS One **12**:e0174165

Klein CC, Alves JMP, Serrano MG, Buck GA, Vasconcelos ATR, Sagot M-F, Teixeira MMG, Camargo EP, Motta MCM (2013) Biosynthesis of vitamins and cofactors in bacterium-harbouring trypanosomatids depends on the symbiotic association as revealed by genomic analyses. PLoS One **8**:e79786

Kořený L, Lukeš J, Oborník M (2010) Evolution of the haem synthetic pathway in kinetoplastid flagellates: An essential pathway that is not essential after all? Int J Parasitol **40**:149–156

Kostygov AY, Butenko A, Nenarokova A, Tashyreva D, Flegontov P, Lukeš J, Yurchenko V (2017) Genome of *Ca.* Pandoraea novymonadis, an endosymbiotic bacterium of the trypanosomatid *Novymonas esmeraldas*. Front Microbiol **8**:1940

Kostygov AY, Dobáková E, Grybchuk-Ieremenko A, Váhala D, Maslov DA, Votýpka J, Lukeš J, Yurchenko V (2016) Novel trypanosomatid-bacterium association: Evolution of endosymbiosis in action. mBio **7**:e01985-01915

Kovarova J, Barrett MP (2016) The pentose phosphate pathway in parasitic trypanosomatids. Trends Parasitol **32**:622–634

Liu B, Liu Y, Motyka SA, Agbo EEC, Englund PT (2005) Fellowship of the rings: the replication of kinetoplast DNA. Trends Parasitol **21**:363–369

López-García P, Eme L, Moreira D (2017) Symbiosis in eukaryotic evolution. J Theor Biol **434**:20–33

Loyola-Machado AC, Azevedo-Martins AC, Catta-Preta CMC, de Souza W, Galina A, Motta MCM (2017) The symbiotic bacterium fuels the energy metabolism of the host trypanosomatid *Strigomonas culicis*. Protist **168**:253–269

Margulis L, Bermudes D (1985) Symbiosis as a mechanism of evolution: status of cell symbiosis theory. Symbiosis **1**:101–124

Marmur J, Cahoon ME, Shimura Y, Vogel HJ (1963) Deoxyribonucleic acid type attributable to a bacterial endosymbiote in the protozoon *Crithidia (Strigomonas) oncopelti*. Nature **197**:1228–1229

Maslov DA, Votypka J, Yurchenko V, Lukes J (2013) Diversity and phylogeny of insect trypanosomatids: all that is hidden shall be revealed. Trends Parasitol **29**:43–52

Maslov DA, Opperdoes FR, Kostygov AY, Hashimi H, Lukes J, Yurchenko V (2019) Recent advances in trypanosomatid research: genome organization, expression, metabolism, taxonomy and evolution. Parasitology **146**:1–27

Motta MCM (2010) Endosymbiosis in trypanosomatids as a model to study cell evolution. Open Parasitol J **4**:139–147

Motta MCM, Catta-Preta CMC, Schenkman S, Martins ACd A, Miranda K, de Souza W, Elias MC (2010) The bacterium endosymbiont of *Crithidia deanei* undergoes coordinated division with the host cell nucleus. PLoS One **5**:e12415

Motta MCM, Martins ACd A, de Souza SSA, Catta-Preta CMC, Silva R, Klein CC, de Almeida LGP, de Lima Cunha O, Ciapina LP, Brocchi M, Colabardini AC, de Araujo Lima B, Machado CR, de Almeida Soares CM, Probst CM, de Menezes CBA, Thompson CE, Bartholomeu DC, Gradia DF, Pavoni DP, Grisard EC, Fantinatti-Garboggini F, Marchini FK, Rodrigues-Luiz GF, Wagner G, Goldman GH, Fietto JLR, Elias MC, Goldman MHS, Sagot M-F, Pereira M, Stoco PH, de Mendonça-Neto RP, Teixeira SMR, Maciel TEF, de

Oliveira Mendes TA, Ürményi TP, de Souza W, Schenkman S, de Vasconcelos ATR (2013) Predicting the proteins of *Angomonas deanei*, *Strigomonas culicis* and their respective endosymbionts reveals new aspects of the Trypanosomatidae family. PLoS One **8**:e60209

Novak E, Haapalainen EF, Da Silva S, Da Silveira JF (1988) Protein synthesis in isolated symbionts from the flagellate protozoon *Crithidia deanei*. J Protozool **35**:375–378

Novy FG, MacNeal WJ, Torrey HN (1907) The trypanosomes of mosquitoes and other insects. J Infect Dis **4**:223–276

Oda LM, Alviano CS, Filho FCS, Angluster J, Roitman I, Souza WD (1984) Surface anionic groups in symbiote-bearing and symbiote-free strains of *Crithidia deanei*. J Protozool **31**:131–134

Parodi-Talice A, Durán R, Arrambide N, Prieto V, Piñeyro MD, Pritsch O, Cayota A, Cerveñansky C, Robello C (2004) Proteome analysis of the causative agent of Chagas disease: *Trypanosoma cruzi*. Int J Parasitol **34**:881–886

Penha LL, Hoffmann L, Souza SSAd, Martins ACd A, Bottaro T, Prosdocimi F, Faffe DS, Motta MCM, Ürményi TP, Silva R (2016) Symbiont modulates expression of specific gene categories in *Angomonas deanei*. Mem Inst Oswaldo Cruz **111**:686–691

Perez-Riverol Y, Csordas A, Bai J, Bernal-Llinares M, Hewapathirana S, Kundu DJ, Inuganti A, Griss J, Mayer G, Eisenacher M, Perez E, Uszkoreit J, Pfeuffer J, Sachsenberg T, Yilmaz S, Tiwary S, Cox J, Audain E, Walzer M, Jarnuczak AF, Ternent T, Brazma A, Vizcaino JA (2019) The PRIDE database and related tools and resources in 2019: improving support for quantification data. Nucleic Acids Res **47**:D442–D450

Posada D (2008) jModelTest: phylogenetic model averaging. Mol Biol Evol **25**:1253–1256

Rodrigues JCF, Godinho JLP, de Souza W (2014) Biology of Human Pathogenic Trypanosomatids: Epidemiology, Lifecycle and Ultrastructure. In Santos ALS, Branquinha MH, d'Avila-Levy CM, Kneipp LF, Sodré CL (eds) Proteins and Proteomics of *Leishmania* and *Trypanosoma*. Springer, Netherlands, Dordrecht, pp 1–42

Ronquist F, Teslenko M, van der Mark P, Ayres DL, Darling A, Hohna S, Larget B, Liu L, Suchard MA, Huelsenbeck JP (2012) MrBayes 3. 2: efficient Bayesian phylogenetic inference and model choice across a large model space. Syst Biol **61**:539–542

Salzman TA, Del C. Batlle AM, Angluster J, de Souza W (1985) Heme synthesis in *Crithidia deanei*: Influence of the endosymbiote. Int J Biochem **17**:1343–1347

Silva FM, Kostygov AY, Spodareva VV, Butenko A, Tossou R, Lukeš J, Yurchenko V, Alves JMP (2018) The reduced genome of *Candidatus* Kinetoplastibacterium sorsogonicusi, the endosymbiont of *Kentomonas sorsogonicus* (Trypanosomatidae): Loss of the haem-synthesis pathway. Parasitology **145**:1287–1293

Teixeira MMG, Borghesan TC, Ferreira RC, Santos MA, Takata CSA, Campaner M, Nunes VLB, Milder RV, de Souza W, Camargo EP (2011) Phylogenetic validation of the genera *Angomonas* and *Strigomonas* of trypanosomatids harboring bacterial endosymbionts with the description of new species of trypanosomatids and of proteobacterial symbionts. Protist **162**:503–524

Turnock DC, Ferguson MAJ (2007) Sugar nucleotide pools of *Trypanosoma brucei*, *Trypanosoma cruzi*, and *Leishmania major*. Eukaryot Cell **6**:1450–1463

Votýpka J, Kostygov AY, Kraeva N, Grybchuk-Ieremenko A, Tesařová M, Grybchuk D, Lukeš J, Yurchenko V (2014) *Kentomonas* gen. n., a new genus of endosymbiont-containing trypanosomatids of Strigomonadinae subfam. n. Protist **165**:825–838

Yurchenko V, Lukeš J (2018) Parasites and their (endo)symbiotic microbes. Parasitology **145**:1261–1264